METHODS

Nicotine dose selection

Nicotine doses of 1 and 3 mg/kg/d were selected based on the literature[1] and took into consideration the fact that blood levels of nicotine and cotinine tend to be lower in pregnant women relative to non-pregnant women due to increased metabolism by liver enzymes.[2,3] For example, the blood nicotine levels of non-pregnant women smoking one pack per day were approximately 30 ng/mL[4] (cotinine levels 267 ng/mL[5]), while pregnant women smoking one pack per day or using a 22 mg/d nicotine patch had nicotine levels of approximately 3-20 ng/mL[6,7] (cotinine levels 100-146 ng/mL[6,8]). In rats, approximately 1 mg/kg/d dose resulted in blood nicotine levels of approximately 5–23 ng/mL (cotinine levels of 182-284 ng/mL);[4,9,10] 3 mg dose resulted in 38 ng/mL nicotine (350 ng/mL cotinine); 6 mg/kg/d resulted in 102 ng/mL nicotine (602 ng/mL cotinine).[11] Therefore, our selected doses of 1 and 3 mg/kg/kg aimed to approximate the use of a nicotine replacement therapy (e.g., a patch) and either regular use of an electronic nicotine delivery system (e.g., vape pen) or a pack-per-day cigarette smoker, respectively.

Histology scoring system definition and discussion

Rat tissues were fixed in 10% buffered formalin for 48 hours then placed in 70% alcohol for fixation. Maternal-fetal units were cross-sectioned and shipped in phosphate buffered saline for paraffin-embedding and hematoxylin and eosin (H&E) -staining (AML labs, Jacksonville, FL). The entirety of each slide was examined at low and high magnification using light microscopy, and the breadth of lesions present in the tissues of the maternal-fetal unit was assessed. Histologic evaluation of inflammation in delivered human placentas has been defined[12-14], particularly pertaining to the umbilical cord, the chorioamnion and the decidua. While umbilical cord inflammation is straightforward in terms of comparison between human and rat, decidual contact with fetal membranes differs over the course of gestation. A modified histopathologic scoring system was implemented based on established methods for human maternal and fetal inflammatory lesions[12,14,16] with consideration for the comparative anatomy[17-23] of the rat and human. Whereas in the late human pregnancy the decidua and chorioamnion are closely apposed surrounding the majority of the amniotic cavity, by gestation day (GD) 18, the rat decidua is discontinuous and the uterine lumen is reestablished except at the mesometrial placental attachment site[15,21]. The non-decidualized endometrial epithelium apposes the inverted yolk sac[18]. Therefore, the staging of maternal inflammatory lesions deviated from the method used for chorioamnionitis in humans. In contrast to humans, there is not a tissue

composed of layered decidua, chorion, and amnion in the rat; we have found the evaluation of the endometrium, the maternal vasculature and blood spaces within the placenta and attachment site, the decidua-yolk sac junction at the outer margins of the placenta, and the parietal and visceral yolk sac membranes, informative of the progression of maternal inflammation in the GD 18 rat.

The data analyzed in the main text are the stage of maternal or fetal inflammation, based on which sites were affected. A site was considered affected if a threshold score of inflammation was met. The score is composed of grade of neutrophil infiltration and/or the number of chronic markers present. To obtain scoring data for each site, slides were assigned a coded identity to blind the histopathologic interpreter as to treatment group. The criteria for evaluating each site are summarized in Table S1. Examples of lesions at select sites appear in Figures S4-S7. Each site was evaluated for neutrophil infiltration and assigned numerical grade (0-2) depending on relative severity, except for yolk sac and Wharton's jelly sites, which were assigned a binary grade depending on presence or absence of neutrophils (0 or 1). Additional lesions associated with chronic changes were noted and were factored into the score for each site. An average of the neutrophil grade and the number of chronic lesions was taken for each site (neutrophil grade + No. of markers of chronicity)/2 to produce a site score, a continuous variable.

To determine which sites represented a stage of inflammatory response, we used the MP only group to represent the standard maternal and fetal inflammatory responses to infection. MP only scores for all sites were analyzed by a principal components analysis (Figure S1). Because score data for the Wharton's jelly, umbilical arteries, umbilical vein, and chorionic vessels were aligned across multiple components, an assumption that these represented the fetal inflammatory response (FIR) was reaffirmed. We therefore performed individual PCA for the remaining sites (Figure S2) as well as for the fetal sites (Figure S3). In the former analysis, the non-fetal variables were in alignment along the first principal component, and we therefore were comfortable grouping them together to represent the maternal inflammatory response (MIR). There were multiple oblique relationships between vectors in the MIR and FIR analyses, so for ease of visualizing the relationships between the variables, an oblique rotation factor analysis was performed for each group (Table S2). Using JMP software version 15.0.0, a quatrimin rotation factor analysis with three factors was performed using the default settings for the MIR data. For the FIR data the same analysis was performed but for four factors; this was done because for the three-factor analysis one variable (Wharton's jelly) was split between two factors; with the four-factor analysis Wharton's jelly was prominently represented by a single factor (the fourth factor did not represent any variable prominently and was disregarded).

This allowed a designation of the variables to stages 0, 1, 2, or 3 of maternal and fetal inflammation (as shown in Figure 1 of the main text). The order of the stages was informed by observation of the patterns of involvement of sites. Cut off points were established to increase specificity of the staging system. The threshold scores for considering whether a site was affected by inflammation and therefore would be counted in the staging of inflammation were determined by optimizing histograms of grade data from Control and MP only groups (data not shown).

RESULTS

Maternal inflammation was impacted by both infection group and placental colonization

The 2-way ANOVA test of data for mean MIR stage indicated a significant contribution to variation of maternal inflammatory response stage among treatment groups by the interaction between nicotine and infection group (Table S7). Figure S8 (top graph) shows individual comparisons of mean MIR stage between the treatment factors, nicotine dose and infection group (sham-inoculated; MP-infected, placental culture-negative; and MP-infected, placenta culture-positive; (*P* values were derived from the Tukey test). Within the MP/PL(+) infection group, MIR stage was significantly lower in the 1 mg/kg/d compared to 3 mg/kg/d (mean and standard deviation, SD: 1.4 ± 0.84 vs 2.2 ± 0.91, *P* = .047); within the 0 mg/kg/d nicotine dose, MIR was significantly lower in the No MP group relative to the MP/PL(+) infection group (1.5 ± 0.90 vs 2.0 ± 0.0, *P* = .04).

Fetal inflammation was impacted by nicotine dose, infection group and placental colonization, and an interaction between the two factors

The 2-way ANOVA test of data for mean FIR stage indicated a significant contribution of infection group (4.4%, *P* =.02), nicotine dose (11.7%, *P* <.001), and an interaction between the two factors (7.0%, *P* =.01; Table S7). Figure S8 (bottom graph) shows individual comparisons of mean FIR stage between the treatment factors, nicotine dose and infection group (sham-inoculated, No MP; MP-infected, placental culture-negative, MP/PL(-); and MP-infected, placenta culture-positive, MP/PL(+);.(*P* values were derived from Tukey multiple comparison tests). FIR was significantly decreased in the 3 mg/kg/d nicotine dose compared to 0 mg/kg/d; (*P* =.01); whereas FIR was significantly increased with the 1 mg/kg/d nicotine dose (P < .02). Simple effects of infection group within a nicotine dose were identified. With the 0 mg/kg/d dose, FIR was increased in MP/PL(-) relative to both No MP and MP/PL(+) (mean ± SD: 1.6 ± 1.4 vs 0.0 ± 0.0, P <.001; and 0.0 ± 0.0, *P* =.01, respectively). Mean FIR was also significantly higher in MP/PL(+) relative to No MP (0.7 ± 1.1 vs 0.0 ± 0.0, *P* =.049). Within the 1 mg/kg/d dose,

FIR was significantly higher in the MP/PL(-) infection group relative to MP/PL(+) (1.6 ± 0.0 vs 0.7 ± 1.1, $P < .01$). Among nicotine doses within infection groups, FIR was significantly higher in the 1 mg/kg/d than other nicotine doses within the No MP group (1.5 ± 1.4 vs 0.0 ± 0.0; $P < .01$). Within the MP/PL(-) infection group, FIR was significantly decreased in the 3 mg/kg/d treated group relative to 0 and 1 mg/kg/d (0.0 ± 0.0 vs 1.6 ± 1.4, $P = .03$, and 0.0 ± 0.0 vs 2.0 ± 1.3, $P = 0.01$). Within the MP/PL(+) group, FIR was significantly decreased in the 3 mg/kg/d group relative to 0 mg/kg/d (0.0 ± 0.0 vs 0.71 ± 1.1, $P = .049$).

Table S1. Scoring criteria for maternal and fetal inflammation.

	Histologic Sites	Acute inflammatory response grades	Markers of chronicity
MIR	Endometrium Decidua	0 = no neutrophil infiltration	Karyorrhexis
	Decidua-yolk sac junction Mesometrial triangle	1 = mild-moderate neutrophil infiltration	Necrosis
	Labyrinth Yolk sac purulent exudate[a]	2 = severe neutrophil infiltration	Fibrin deposition
FIR	Chorionic vessels Umbilical vein	0 = no vasculitis 1 = acute vasculitis	Karyorrhexis Necrosis
	Umbilical arteries Wharton's jelly[b]	2 = prolonged / necrotizing vasculitis	Fibrin deposition Concentric vasculitis

Histologic sites for maternal (MIR) and fetal (FIR) inflammatory responses. Each site was evaluated and was signed an individual acute inflammatory response grade, and the presence of chronic inflammatory response lesions was noted. The acute inflammation numeric grade and the numeric count of chronic lesion markers for each site were given equal weight and were averaged to produce a final score for each site.

[a,b]Binary grades (0 = absent, 1 = present) were assigned for [a]neutrophilic exudate associated with the luminal surface of the inverted yolk sac, and for [b]neutrophilic infiltration into Wharton's jelly beyond perivascular areas; markers of chronicity were not counted for these sites.

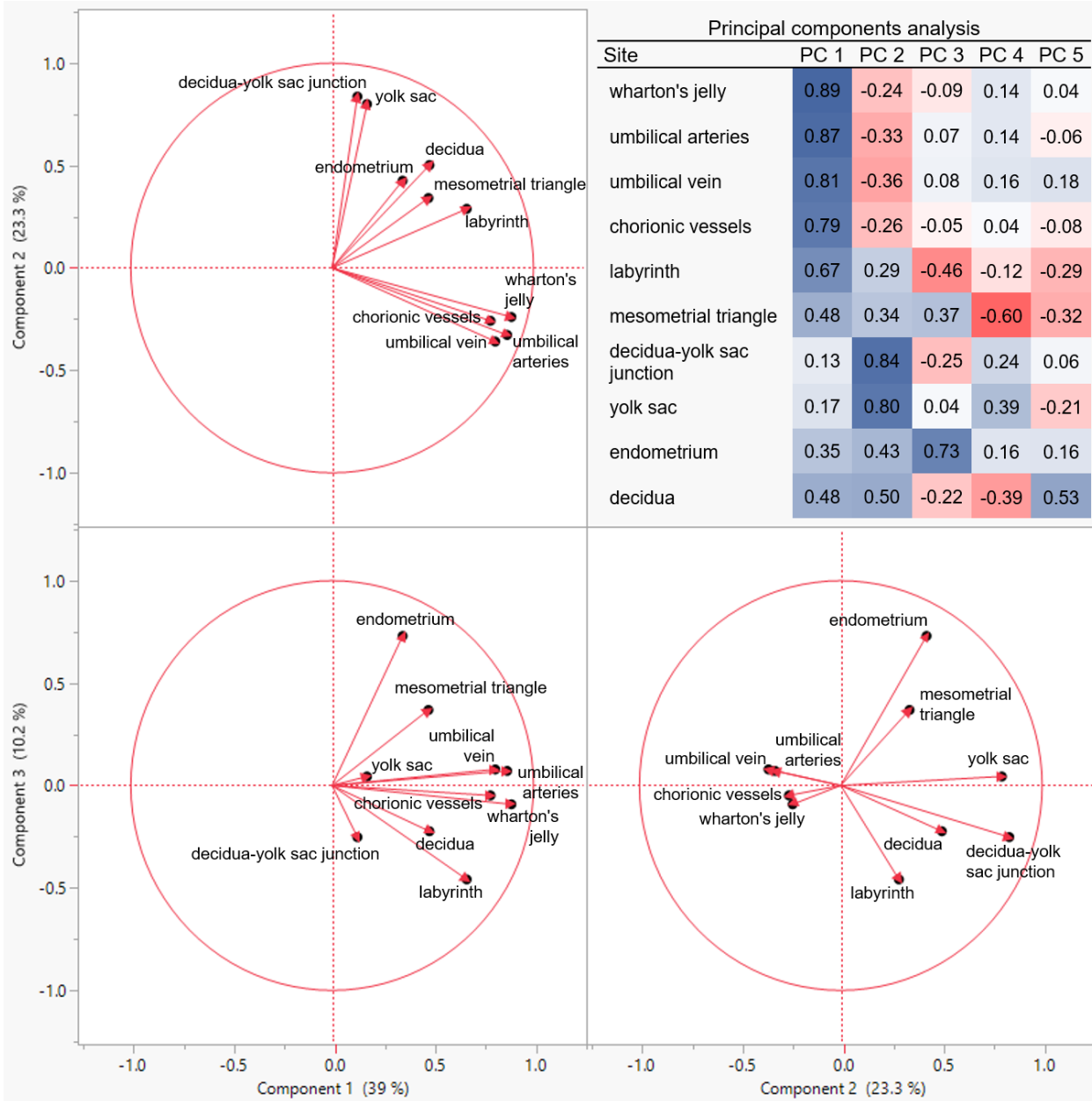| Principal components analysis					
Site	PC 1	PC 2	PC 3	PC 4	PC 5
wharton's jelly	0.89	-0.24	-0.09	0.14	0.04
umbilical arteries	0.87	-0.33	0.07	0.14	-0.06
umbilical vein	0.81	-0.36	0.08	0.16	0.18
chorionic vessels	0.79	-0.26	-0.05	0.04	-0.08
labyrinth	0.67	0.29	-0.46	-0.12	-0.29
mesometrial triangle	0.48	0.34	0.37	-0.60	-0.32
decidua-yolk sac junction	0.13	0.84	-0.25	0.24	0.06
yolk sac	0.17	0.80	0.04	0.39	-0.21
endometrium	0.35	0.43	0.73	0.16	0.16
decidua	0.48	0.50	-0.22	-0.39	0.53

Figure S1. Principal components analysis (PCA) of all sites scored for inflammation. Loading plots for principal components (PC) 1-3 are shown. The table shows the formatted loading matrix for PC 1-5. A continuous color scale was applied, with red for values of -1, white for values of 0, and blue for values of +1. Wharton's jelly, umbilical arteries, umbilical vein, and chorionic vessels are aligned across PC 1-3. That is, all are high-positive in PC 1 (as best demonstrated in the top left plot); low-negative in PC 2 (bottom right plot), and zero (defined as -0.1 through +0.1) in PC 3 (bottom left plot).
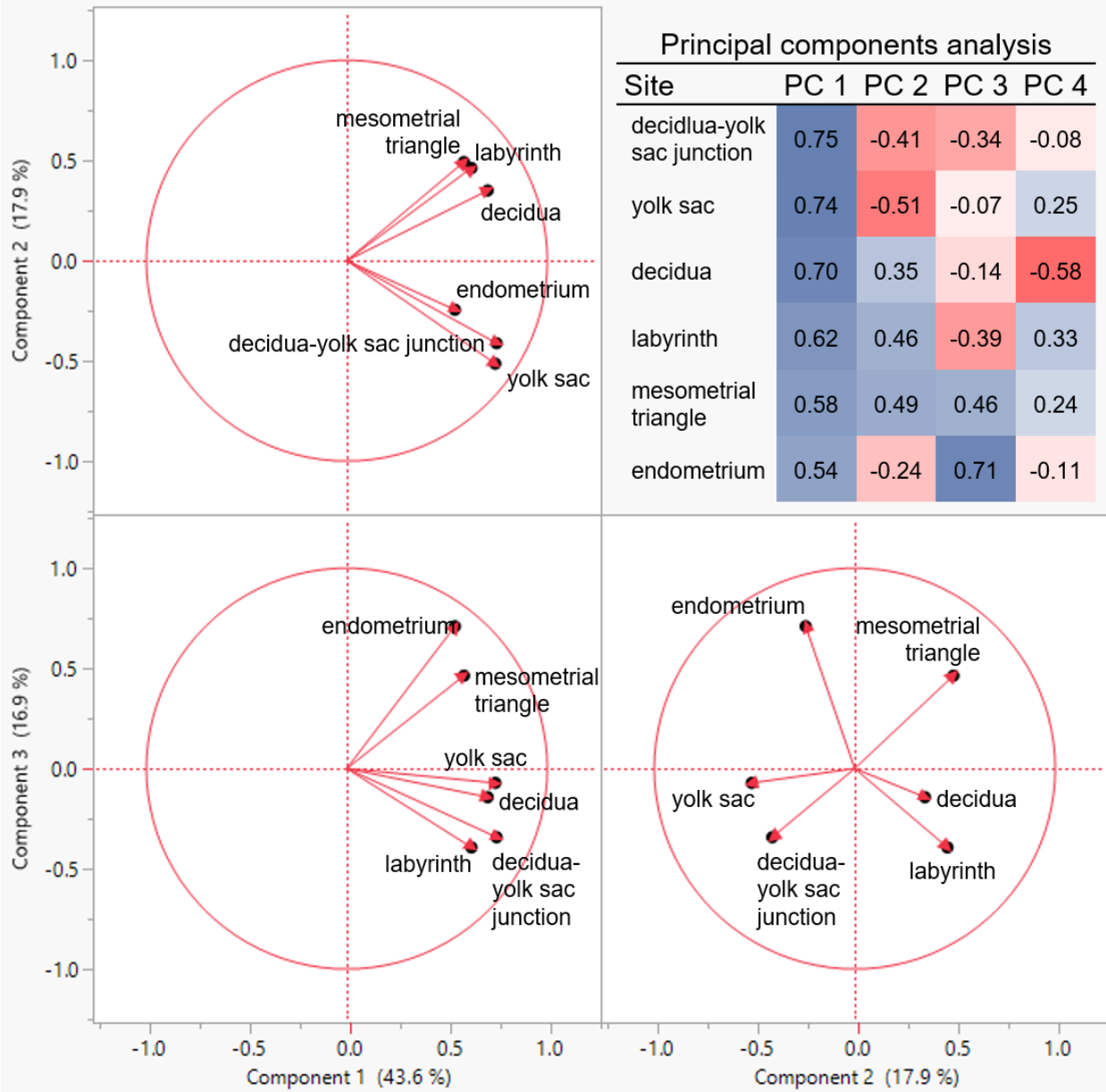
Principal components analysis

Site	PC 1	PC 2	PC 3	PC 4
decidlua-yolk sac junction	0.75	-0.41	-0.34	-0.08
yolk sac	0.74	-0.51	-0.07	0.25
decidua	0.70	0.35	-0.14	-0.58
labyrinth	0.62	0.46	-0.39	0.33
mesometrial triangle	0.58	0.49	0.46	0.24
endometrium	0.54	-0.24	0.71	-0.11

Figure S2. PCA of maternal sites scored for inflammation. Loading plots for principal components (PC) 1-3 are shown. The table shows the formatted loading matrix for PC 1-4. A continuous color scale was applied, with red for values of -1, white for values of 0, and blue for values of +1. The relationship between variables is not easily interpreted and may more appropriately be assessed by an oblique rotated factor analysis (see Table S2).
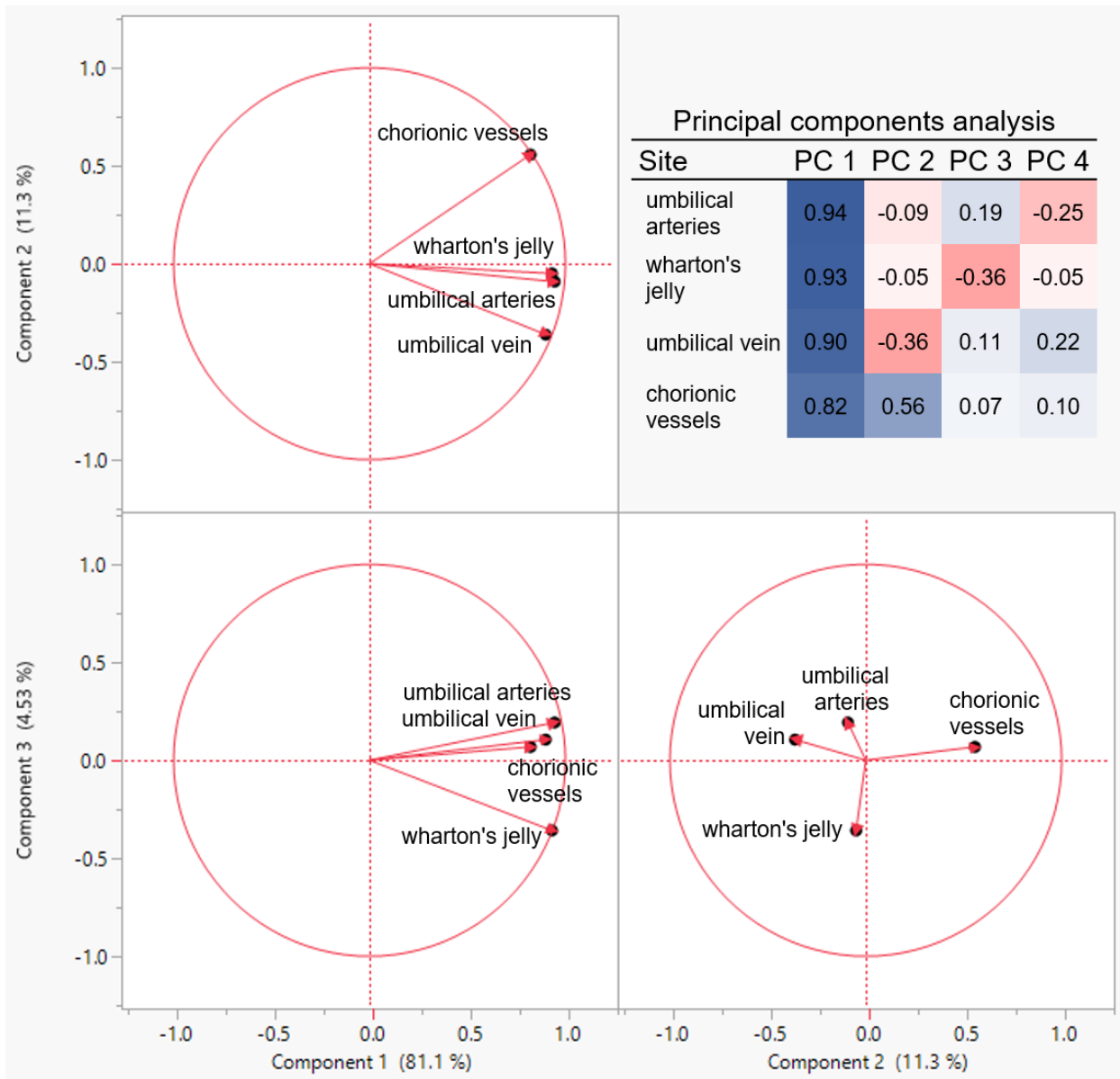
Figure S3. PCA of fetal sites scored for inflammation. Loading plots for principal components (PC) 1-3 are shown. The table shows the formatted loading matrix for PC 1-4. A continuous color scale was applied, with red for values of -1, white for values of 0, and blue for values of +1. The relationship between variables is not easily interpreted and may more appropriately be assessed by an oblique rotated factor analysis (see Table S2).

Table S2. Factor analysis of maternal and fetal sites.

Maternal site	Factor 1	Factor 2	Factor 3
Decidua-yolk sac junction	1.00	0.01	-0.06
Yolk sac exudate	0.62	0.06	0.19
Labyrinth	0.07	0.69	-0.18
Mesometrial triangle	-0.13	0.59	0.24
Decidua	0.20	0.57	0.01
Endometrium	0.13	0.00	0.97
Fetal site	Factor 1	Factor 2	Factor 3
Umbilical vein	0.97	0.00	-0.03
Umbilical arteries	0.77	0.05	0.11
Wharton's jelly	0.00	0.94	0.00
Chorionic vessels	0.00	0.00	0.89

A quartimin rotated factor analysis was performed. Maternal and fetal sites were analyzed separately. The rotated factor loading matrix for each analysis is shown. A continuous color scale was applied, with red for values of -1, white for values of 0, and blue for values of +1. The analyses of the two groups of variables (maternal and fetal, as indicated by PCA) yielded a clear alignment of variables that formed the basis of the staging system. Maternal inflammatory response (MIR): Stage 1 = endometrium score; Stage 2 = average of labyrinth, mesometrial, and decidua scores; Stage 3: averaged decidua-yolk sac junction and parietal/visceral yolk sac membrane scores. Fetal inflammatory response (FIR): Stage 1 = chorionic vessels score; Stage 2 = average of umbilical vein and arteries scores; Stage 3 = Wharton's jelly score.
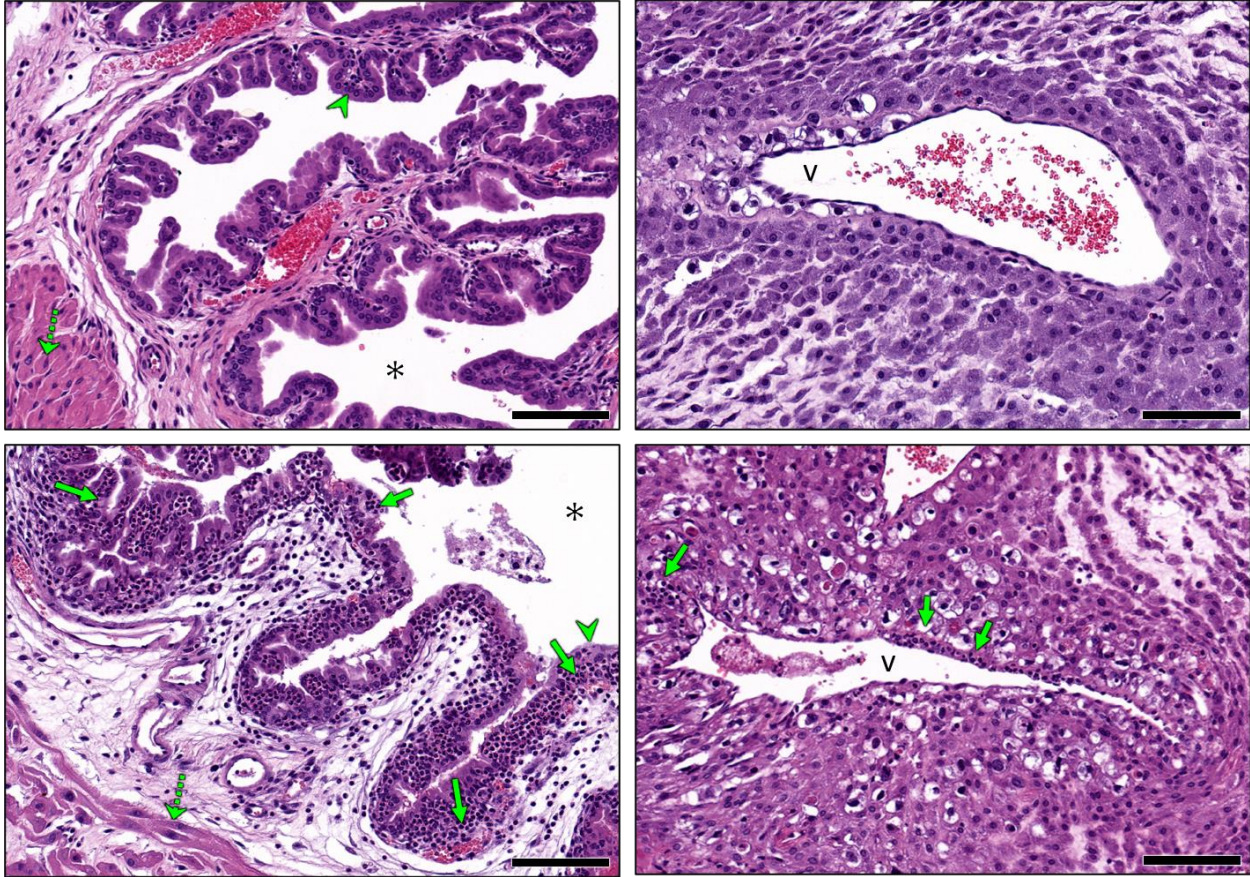
Figure S4. Lesions indicative of Stage 1 (left) and Stage 2 (right) MIR. Normal endometrium; (Control, top left) and endometrium and with leukocyte infiltration into the epithelial cell layer (MP only, bottom left panel). Myometrium (dotted arrow) underlies the submucosa, submucosa which appears expanded in the bottom panel. Epithelium (arrowhead) lines mucosal folds, which project into the uterine lumen (asterisk, *). Leukocytes, primarily polymorphonuclear cells (PMN), have infiltrated the mucosal layer (bottom image, solid arrows). Uterine vessel (v) within the mesometrial triangle; normal (Control, top right) and with leukocyte infiltrates (MP only, solid arrows, bottom). Photomicrographs were captured by ImageScope software from H&E-stained slides scanned using Aperio equipment; scale bars are 100 μm.
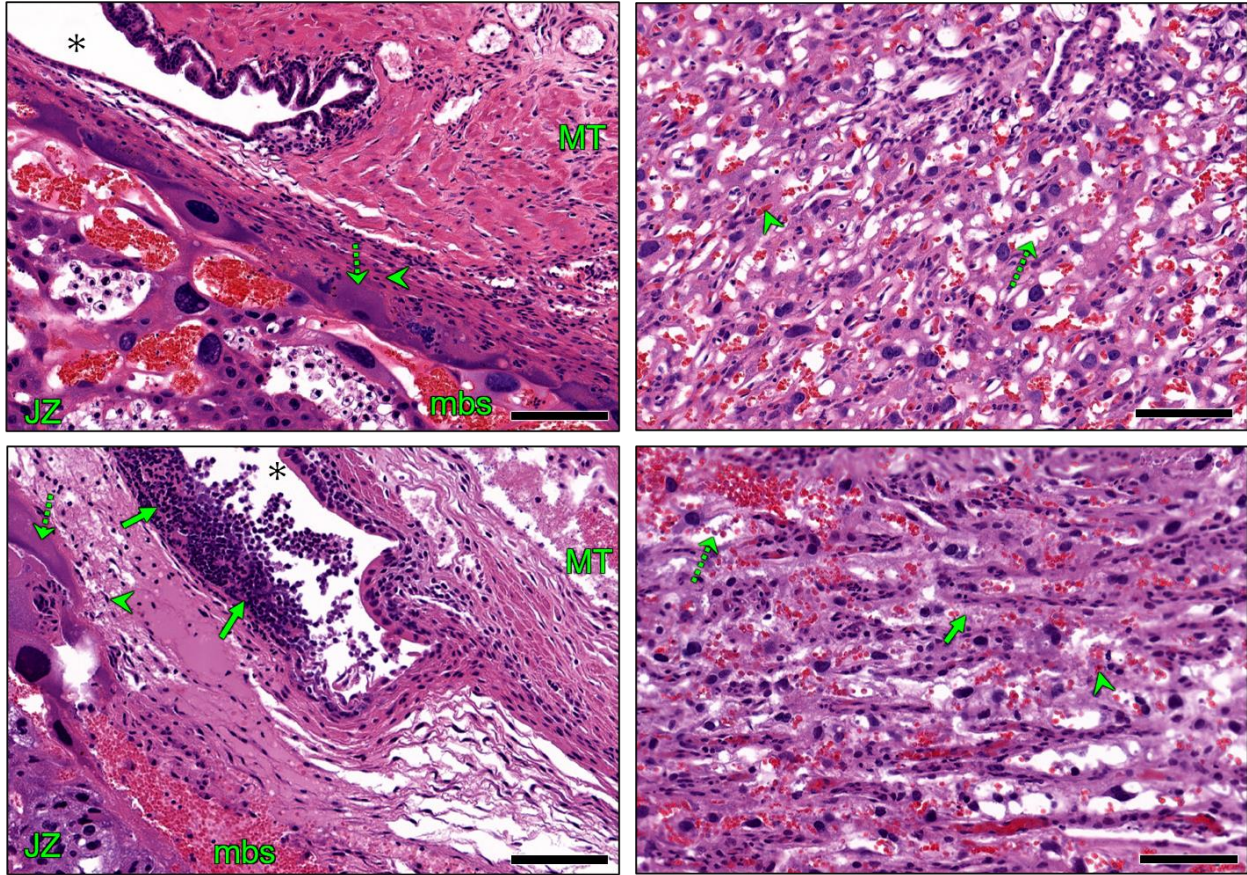
Figure S5. Lesions indicative of Stage 2 MIR. Top left: dense, well organized decidual cells (arrowhead) form a compact layer with a tight association to both mesometrial triangle (MT) and the trophoblast giant cells (dotted arrow) of the junctional zone (JZ); Low NIC only. Bottom left: loose, necrotic decidua with adherence of PMNs at the luminal surface of the decidua. The attachment between maternal (MT) and fetal (JZ) components of the unit is weakened. The trophoblast lining of the maternal blood spaces (mbs) is obliterated; Mid NIC + MP. Top right: Normal labyrinth (Control), showing maternal blood spaces (dotted arrow) and fetal capillary (arrowhead); bottom right: labyrinth with fibrinous debris in the maternal blood spaces (solid arrow); Low NIC + MP. Chorionic tissue separates maternal and fetal blood. Photomicrographs were captured by ImageScope software from H&E-stained slides scanned using Aperio equipment; scale bars are 100 µm.
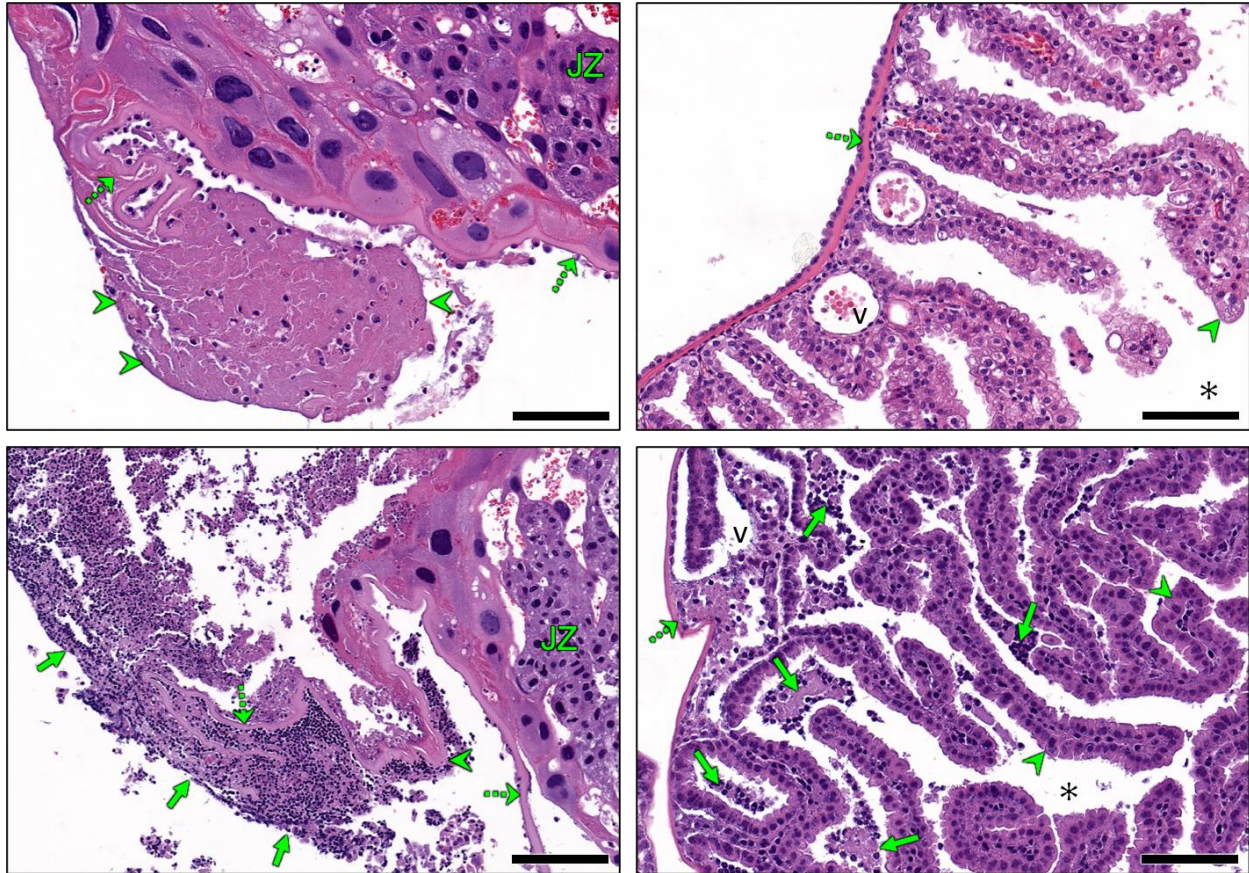
Figure S6. Stage 3 MIR: Parietal yolk sac (PYS) remnant; normal (Control, top), and with purulent exudate (Mid NIC + MP, bottom). In the rat, the yolk sac ruptures on gestation day (GD) 16. At GD 18, we see the retracted parietal yolk sac remnant (arrowheads), and Reichert's membrane (dotted arrows), a thick basement membrane that lines the placental disk (of which the junctional zone (JZ) is visible) layered by endodermal cells. The endodermal cells are visible as dark nuclei lining the placental disk and also in the retracted parietal yolk sac remnant. The bottom figure shows Reichert's membrane lifted from is attachment to the chorionic portion of the labyrinth (dotted line, large arrowhead). Large numbers of polymorphonuclear cells (PMN) are aggregated around the retracted parietal yolk sac remnant (solid arrows). The origin of these PMNs (e.g., maternal, fetal, embryonic tissue, an adjacent maternal-fetal unit) is not known. Endodermal cells lining Reichert's membrane have been sloughed. Scale bar is 100 μm. Visceral yolk sac (VYS), normal (Control, top), and with mucopurulent exudate and vascular luminal debris (MP only, bottom). At GD 18, the VYS epithelium of endodermal origin (arrowheads) faces the uterine lumen, while the mesoderm (dotted arrow) faces the amnion. Vitelline vessels (v) are involved in carrying histiotrophic nutrition moving from the endometrial epithelium to VYS epithelium, to the fetal circulation. In the bottom image, spaces between villi that are contiguous with the uterine lumen are occupied by mucopurulent exudate (solid arrows). Effacement of the endothelium and luminal debris is observed in the vessel (v), and mesodermal cells seen in the top image (dotted arrow) are absent in the bottom figure. Photomicrographs were captured by ImageScope software from H&E-stained slides scanned using Aperio equipment; scale bars are 100 μm.
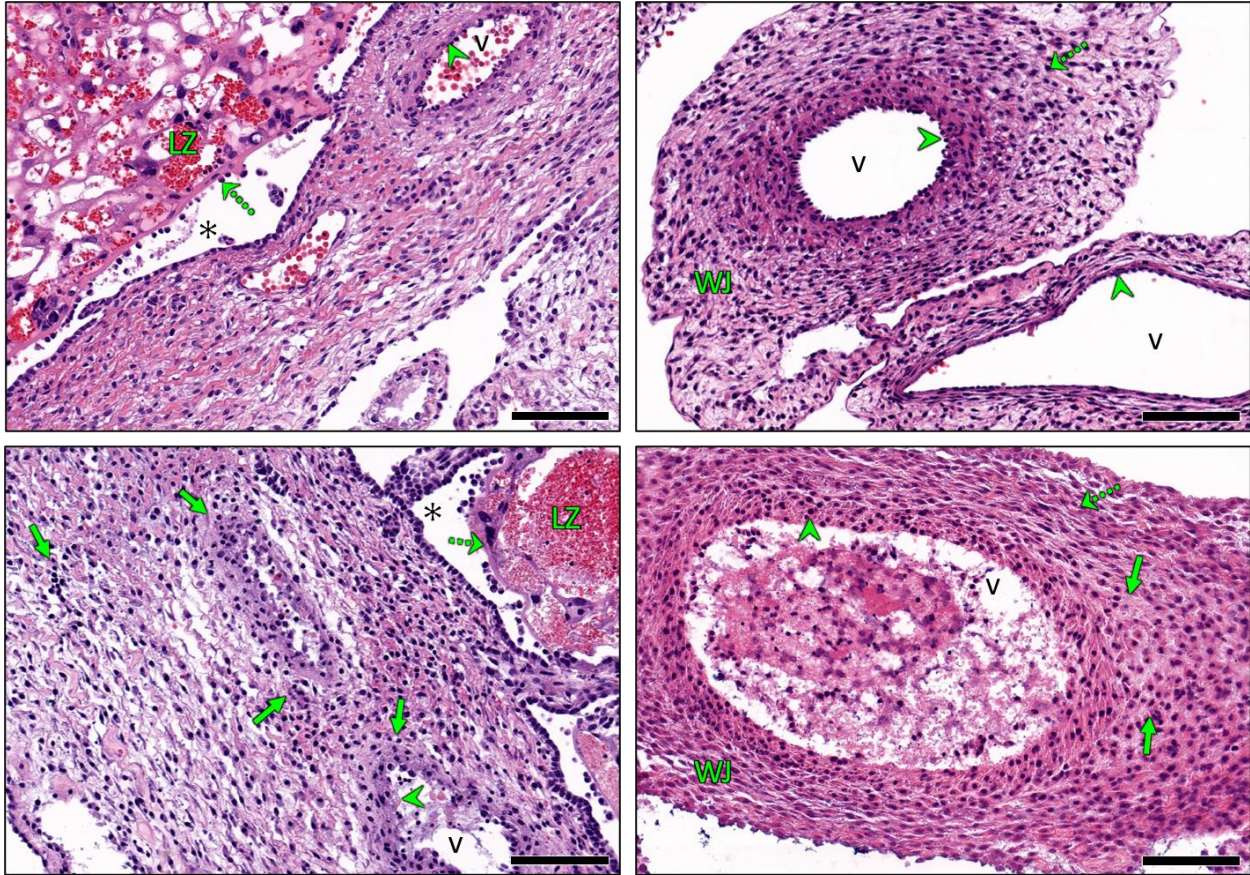
Figure S7. FIR: Chorionic plate; normal (Control, top), and with leukocyte infiltration (Mid NIC + MP, bottom). The lumen of the uterus is contiguous with the intraplacental parietal yolk sac lumen (*); within the placenta the PYS is bounded by Reichert's membrane (dotted arrows) which lines the placental disk (the labyrinth zone (LZ) is visible here) and the epithelium-lined chorionic plate. Chorionic vessels (v) are lined by fetal (allantoic) endothelium (arrowhead). These vessels carry fetal blood to and from the fetal capillaries in the labyrinth zone, where exchange with maternal blood occurs. The bottom figure shows PMN infiltration (solid arrows) into the chorionic plate stroma adjacent to chorionic vessels, of which the endothelium is degraded in the bottom figure (arrowhead). Umbilical cord, normal (Low NIC only, top), and with leukocyte infiltration and endothelial effacement (Low NIC only, bottom). The Wharton's jelly (WJ) consists of fibroblast-like cells (dotted arrows) and connective tissue. Vessels (v) are lined by endothelium (arrowhead). In the bottom image, leukocytes have infiltrated the connective tissue, which appears fragmented (solid arrows). The fibroblast nuclei are pale and there is loss of definition in their appearance (dotted arrow). The endothelium is absent (arrowhead) and the vessel (v) is filled with cellular debris and fibrinous material. All photomicrographs: Hematoxylin and eosin (H&E) stain. Image captured by ImageScope software viewing an Aperio-scanned slide. Scale bar is 100 μm.
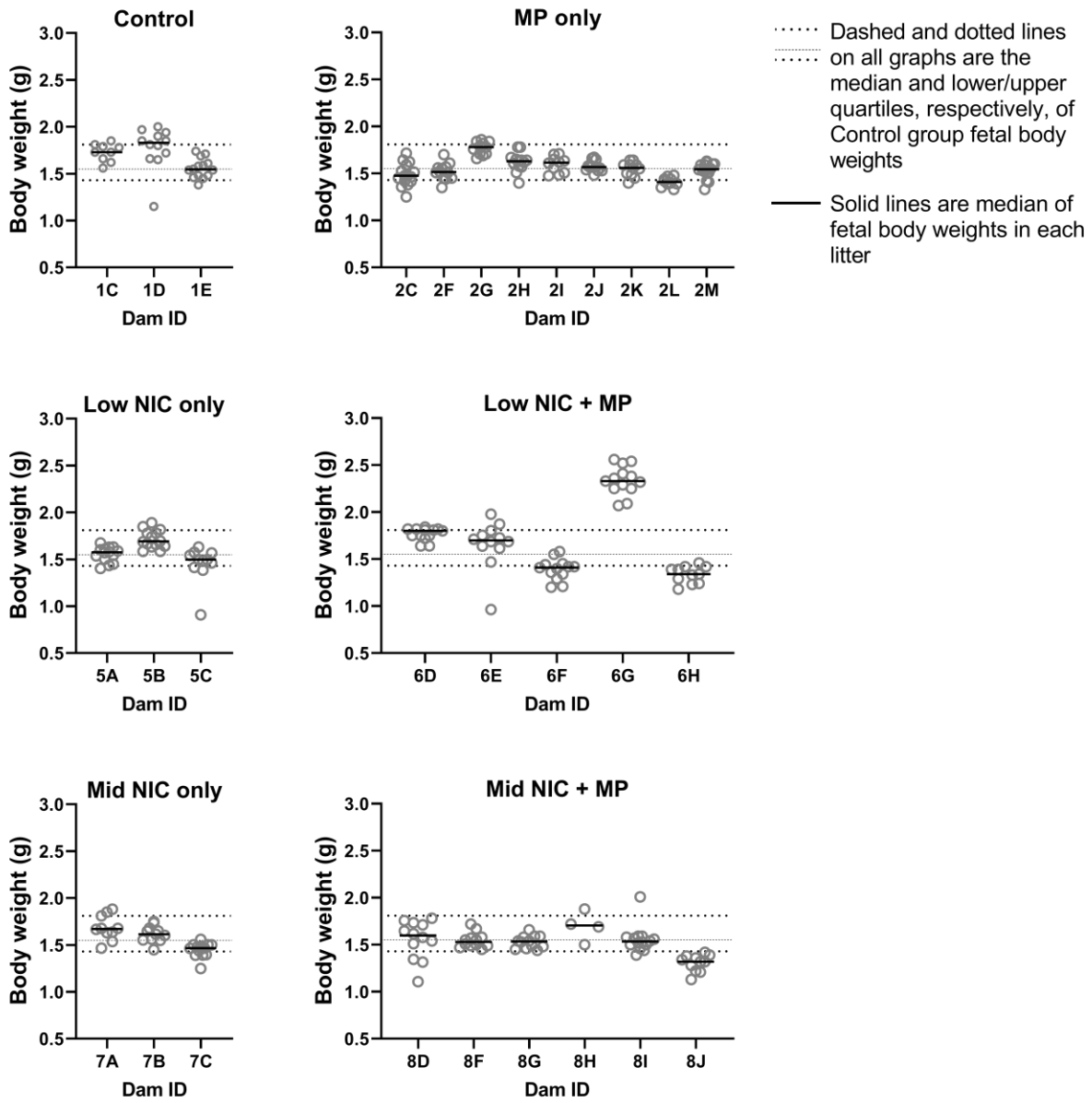
Figure S8. Fetal body weights were variable in the Low NIC + MP group. Open circles are the individual fetus body weights in grams and solid lines are median body weight for each litter, grouped and identified by Dam ID. The dashed and dotted lines on all graphs are the median and upper/lower quartiles for the Control group. Individual Kruskal-Wallis tests for each treatment group indicated significant variation among litters in all treatment groups ($P < .001$ for each treatment group). The Kruskal-Wallis and Dunn's tests were performed comparing median of body weights pooled across each treatment group with the Control group, and results are presented in Table 1 of the main text. Because the Dam 6G litter seems unusually large, we also performed Kruskal-Wallis and Dunn's tests with this litter omitted. While with the 6G litter included the Low NIC + MP group median fetal weight was not different from the Control group median fetal weight (Table 1), with this litter omitted the Low NIC + MP group median fetal weight in grams (median = 1.55; 1st and 3rd quartiles = 1.38 and 1.75) was significantly lower ($P = .006$) than Controls (median = 1.69; 1st and 3rd quartiles = 1.55 and 1.81), similar to the other infected groups

Table S3. Relative risks (RR) for colonization of intrauterine sites between treatments.

Risk between treatments of *M. pulmonis* culture-positive **endometrium**			
Reference group (n)	Comparison group (n)	RR (95% CI)	Fisher exact test *P* value
MP only (9)	Low NIC + MP (5)	**0.00 (0.00 to 0.73)**	**0.03**
	Mid NIC + MP (6)	0.00 (0.00 to 1.00)	>0.999
Mid NIC + MP (6)	Low NIC + MP (5)	**0.25 (0.08 to 0.83)**	0.06
Risk between treatments of *M. pulmonis* culture-positive **placenta**			
Reference group	Comparison group	RR (95% CI)	Fisher exact test *P* value
MP only (111)	Low NIC + MP (62)	**0.74 (0.58 to 0.93)**	**0.01**
	Mid NIC only (65)	1.03 (0.81 to 1.29)	0.87
Mid NIC only (65)	Low NIC + MP (62)	**0.62 (0.42 to 0.89)**	**0.01**
Risk between treatments of *M. pulmonis* culture-positive **amniotic fluid**			
Reference group	Comparison group	RR (95% CI)	Fisher exact test *P* value
MP only (109)	Low NIC + MP (62)	**0.69 (0.56 to 0.86)**	**<0.01**
	Mid NIC only (63)	1.08 (0.86 to 1.40)	0.62
Mid NIC only (63)	Low NIC + MP (62)	**0.41 (0.21 to 0.72)**	**<0.01**

Sample sizes for each subgroup are indicated by (n) for each comparison. Statistically significant values (RR with 95% confidence intervals (CI) above or below, but not spanning 1; *P* values derived from Fisher's exact test <0.05) appear in bold.

Table S4. Relative risks for moderate-to-advanced inflammation versus none-to-early inflammation between treatments in sham-inoculated and MP-infected groups.

Risk between treatments of moderate to advanced **maternal** inflammatory response **(MIR)**			
Reference group (n)	Comparison group (n)	RR (95% CI)	Fisher exact test *P* value
Control (26)	MP only (49)	1.72 (0.91 to 3.05)	0.12
	Low NIC only (13)	**1.81 (1.24 to 2.40)**	**0.02**
	Mid NIC only (11)	0.92 (0.71 to 1.41)	0.73
Mid NIC only (11)	Low NIC only (13)	**≥ 1.50 (1.50 to infinity)**	**0.01**
MP only (49)	Low NIC + MP (22)	0.81 (0.49 to 1.16)	0.37
	Mid NIC + MP (31)	0.95 (0.56 to 1.38)	>0.999
Low NIC + MP (22)	Mid NIC + MP n = 31	1.30 (0.63 to 2.38)	0.53
Risk between treatments of moderate to advanced **fetal** inflammatory response **(FIR)**			
Reference group	Comparison group	RR (95% CI)	Fisher exact test *P* value
Control (18)	MP only (49)	**≥ 2.00 (2.00 to infinity)**	**<0.01**
	Low NIC only (16)	**≥ 2.00 (2.00 to infinity)**	**<0.001**
	Mid NIC only (8)	infinity (< 0.001 to infinity)	>0.999
Mid NIC only (8)	Low NIC only (16)	**2.14 (1.33 to 4.03)**	**0.01**
MP only (49)	Low NIC + MP (22)	1.22 (0.89 to 1.77)	0.30
	Mid NIC + MP (21)	**0.59 (0.45 to 0.73)**	**<0.001**
Low NIC + MP (22)	Mid NIC + MP (21)	**0.32 (0.19 to 0.50)**	**<0.001**

Outliers in the MIR and FIR stage data were identified by the ROUT method (Q = 1%) and eliminated prior to analyses in tables S4 through S6. Sample sizes for each subgroup are indicated by (n) for each comparison. Statistically significant values (RR with 95% confidence intervals (CI) above or below, but not spanning 1; *P* values derived from Fisher's exact test <0.05) appear in bold. Note that for comparisons between Low NIC and Mid NIC groups they may appear in either reference or comparison columns; depending on the comparison of interest.

Table S5. Impact of maternal and fetal inflammatory responses on relative risk for placental and amniotic fluid colonization.

Risk for *M. pulmonis* colonization of placenta and amniotic fluid with **high MIR**			
Treatment	Site of colonization (n)	RR (95% CI)	Chi-square *P* value
MP only	Placenta (47)	1.18 (0.39 to 3.34)	.78
	Amniotic fluid (30)	1.73 (0.45 to 6.43)	.45
Low NIC + MP	Placenta (22)	**0.14 (0.02 to 0.69)**	**< .01**
	Amniotic fluid (10)	2.14 (0.64 to 12.04)	0.26
Mid NIC + MP	Placenta (20)	3.11 (0.90 to 10.43)	.074
	Amniotic fluid (30)	1.25 (0.17 to 7.83)	0.84
Risk for *M. pulmonis* colonization of placenta and amniotic fluid **with high FIR**			
Treatment	Site of colonization (n)	RR (95% CI)	Chi-square *P* value
MP only	Placenta (47)	**0.56 (0.29 to 0.95)**	**.03**
	Amniotic fluid (30)	**0.51 (0.24 to 0.86)**	**< .01**
Low NIC + MP	Placenta (22)	**0.38 (0.12 to 0.93)**	**.03**
	Amniotic fluid (10)	0.57 (0.23 to 1.47)	0.18
Mid NIC + MP	Placenta (20)	1.00 (0.44 to 1.23)	NA
	Amniotic fluid (17)	1.00 (0.51 to 1.30)	NA

Outliers in the MIR and FIR stage data were identified by the ROUT method (Q = 1%) and eliminated prior to analyses in tables S4 through S6. Sample sizes for each subgroup are indicated by (n) for each comparison. Statistically significant values (RR with 95% confidence intervals (CI) above or below, but not spanning 1; *P* values derived from Chi-square <0.05) appear in bold.

S<small>UPPLEMENT REFERENCES</small>

1. Hussein J, Farkas S, MacKinnon Y, Ariano RE, Sitar DS, Hasan SU. Nicotine dose-concentration relationship and pregnancy outcomes in rat: biologic plausibility and implications for future research. *Toxicol Appl Pharmacol.* 2007;218(1):1-10.
2. Benowitz NL, Hukkanen J, Jacob P, 3rd. Nicotine chemistry, metabolism, kinetics and biomarkers. *Handb Exp Pharmacol.* 2009(192):29-60.
3. Dempsey D, Jacob P, 3rd, Benowitz NL. Accelerated metabolism of nicotine and cotinine in pregnant smokers. *J Pharmacol Exp Ther.* 2002;301(2):594-598.
4. Polli FS, Kohlmeier KA. Prenatal nicotine exposure in rodents: why are there so many variations in behavioral outcomes? *Nicotine Tob Res.* 2019.
5. Foulds J, Hobkirk A, Wasserman E, et al. Estimation of compliance with exclusive smoking of very low nicotine content cigarettes using plasma cotinine. *Prev Med.* 2018;117:24-29.
6. Ogburn PL, Jr., Hurt RD, Croghan IT, et al. Nicotine patch use in pregnant smokers: nicotine and cotinine levels and fetal effects. *Am J Obstet Gynecol.* 1999;181(3):736-743.
7. Selby P, Hackman R, Kapur B, Klein J, Koren G. Heavily smoking women who cannot quit in pregnancy: evidence of pharmacokinetic predisposition. *Ther Drug Monit.* 2001;23(3):189-191.
8. Mamsen LS, Jonsson BAG, Lindh CH, et al. Concentration of perfluorinated compounds and cotinine in human foetal organs, placenta, and maternal plasma. *Sci Total Environ.* 2017;596-597:97-105.
9. Fewell JE, Smith FG, Ng VK. Threshold levels of maternal nicotine impairing protective responses of newborn rats to intermittent hypoxia. *J Appl Physiol (1985).* 2001;90(5):1968-1976.
10. Fung YK, Lau YS. Effects of prenatal nicotine exposure on rat striatal dopaminergic and nicotinic systems. *Pharmacol Biochem Behav.* 1989;33(1):1-6.
11. Richardson SA, Tizabi Y. Hyperactivity in the offspring of nicotine-treated rats: role of the mesolimbic and nigrostriatal dopaminergic pathways. *Pharmacol Biochem Behav.* 1994;47(2):331-337.
12. Kim CJ, Romero R, Chaemsaithong P, Chaiyasit N, Yoon BH, Kim YM. Acute chorioamnionitis and funisitis: definition, pathologic features, and clinical significance. *Am J Obstet Gynecol.* 2015;213(4 Suppl):S29-52.
13. Redline RW. Inflammatory responses in the placenta and umbilical cord. *Semin Fetal Neonatal Med.* 2006;11(5):296-301.
14. Redline RW. Classification of placental lesions. *Am J Obstet Gynecol.* 2015;213(4 Suppl):S21-28.
15. Welsh AO, Enders AC. Occlusion and reformation of the rat uterine lumen during pregnancy. *Am J Anat.* 1983;167(4):463-477.
16. Redline RW. Inflammatory response in acute chorioamnionitis. *Semin Fetal Neonatal Med.* 2012;17(1):20-25.
17. Carter AM. Animal models of human placentation--a review. *Placenta.* 2007;28 Suppl A:S41-47.
18. Carter AM, Enders AC. Placentation in mammals: Definitive placenta, yolk sac, and paraplacenta. *Theriogenology.* 2016;86(1):278-287.
19. Clark DA. The use and misuse of animal analog models of human pregnancy disorders. *J Reprod Immunol.* 2014;103:1-8.
20. Fonseca BM, Correia-da-Silva G, Teixeira NA. The rat as an animal model for fetoplacental development: a reappraisal of the post-implantation period. *Reprod Biol.* 2012;12(2):97-118.
21. Furukawa S, Kuroda Y, Sugiyama A. A comparison of the histological structure of the placenta in experimental animals. *J Toxicol Pathol.* 2014;27(1):11-18.
22. Georgiades P, Ferguson-Smith AC, Burton GJ. Comparative developmental anatomy of the murine and human definitive placentae. *Placenta.* 2002;23(1):3-19.
23. Soares MJ, Chakraborty D, Karim Rumi MA, Konno T, Renaud SJ. Rat placentation: an experimental model for investigating the hemochorial maternal-fetal interface. *Placenta.* 2012;33(4):233-243.